

NACA TN 4344 98907

0067227



TECH LIBRARY KAFB, NM

NATIONAL ADVISORY COMMITTEE FOR AERONAUTICS

TECHNICAL NOTE 4344

PERFORMANCE AT LOW SPEEDS OF COMPRESSOR ROTORS HAVING
LOW-CAMBERED NACA 65-SERIES BLADES WITH HIGH
INLET ANGLES AND LOW SOLIDITIES

By James C. Emery and Paul W. Howard

Langley Aeronautical Laboratory
Langley Field, Va.



Washington
August 1958

AFMDC
TECHNICAL LIBRARY

NATIONAL ADVISORY COMMITTEE FOR AERONAUTICS



0067227

TECHNICAL NOTE 4344

PERFORMANCE AT LOW SPEEDS OF COMPRESSOR ROTORS HAVING
LOW-CAMBERED NACA 65-SERIES BLADES WITH HIGH
INLET ANGLES AND LOW SOLIDITIES

By James C. Emery and Paul W. Howard

SUMMARY

Three compressor rotors having low-cambered 6-percent-thick NACA 65-series blade sections were tested at low speeds. The tests were made at solidities of 0.5, 0.75, and 1.0, without guide vanes or stators, over ranges of blade-setting angles and quantity-flow rates.

The rotor operated with an overall efficiency greater than 80 percent for all solidities over a moderate range of angles of attack for all blade-setting angles. The measured blade-element performance is compared with performance estimated from two-dimensional cascade data in order to extend the correlation of cascade and compressor-rotor data over an inlet-angle range from 64° to 76° . The comparison indicates that the measured rotor turning angles were within $\pm 2^\circ$ of those predicted from cascade data.

INTRODUCTION

Multistage axial-flow compressors are designed, in general, for constant axial velocity and, when used as a part of the modern jet engine, require a short diffuser and/or a stator blade between the last stage and the combustion chamber to reduce the velocity to practical limits. If the absolute velocity leaving the last-stage rotor could be sufficiently reduced by operating the later stages of the multistage compressor at higher inlet angles and lower axial velocity, then air might be introduced more directly into the combustion chamber. In order to determine if this operation is practical, detailed design data of reference 1 have been supplemented by low-speed two-dimensional data reported in reference 2 for thin low-cambered NACA 65-series blade sections at high inlet angles and low solidities.

Flow through a two-dimensional cascade is somewhat different from that through rotating blade rows; therefore, a correlation is needed

between the simpler two-dimensional cascade flows and the flow through a rotating compressor. Performance data of three rotors were obtained for three blade-setting angles and for solidities of 0.5, 0.75, and 1.0 for a range of inlet angles from 64° to 76° by using NACA 65- $(c_{l_0}A_{10})06$ blade sections (where c_{l_0} is the design lift coefficient of an isolated airfoil, as in ref. 2), and a comparison is made with two-dimensional data of reference 2.

SYMBOLS

c_{l_0}	design lift coefficient of isolated airfoil
D	diameter, ft
M	mass flow, slugs/sec
n	rotor speed, rps
p	static pressure, lb/sq ft
p_t	total pressure, lb/sq ft
Q	quantity flow of air, cu ft/sec
r	radius, in.
U	rotor-blade velocity, ft/sec
V	absolute velocity of air, ft/sec
α	angle of attack relative to blade chord, deg
β	air-inlet angle relative to blade, measured from axis, deg
η	adiabatic efficiency, $\frac{(p_{t,2} - p_{t,1})}{2\pi n M \left(\frac{r}{12}\right) \Delta V_\theta}$, percent
θ	air turning angle, deg
ξ	blade-setting angle, angle between blade chord and rotor axis, deg
ρ	air density, slugs/cu ft

σ	solidity, ratio of blade chord to gap
Φ	quantity-flow coefficient, $\frac{Q}{nD_t^3}$
ψ	pressure-rise coefficient
ψ_s	static-pressure-rise coefficient, $\frac{(p_2 - p_1)}{\frac{1}{2}\rho U_t^2}$
ψ_t	total-pressure-rise coefficient, $\frac{(p_{t,2} - p_{t,1})}{\frac{1}{2}\rho U_t^2}$

Subscripts:

1	upstream of blade row
2	downstream of blade row
d	design condition
m	mean-radius section
R	relative to rotor
t	tip section
θ	tangential

ROTOR DESIGN AND TEST PROGRAM

The rotors used in this investigation were designed with an exit tangential velocity distribution inversely proportional to the length of the radius (free-vortex condition) by using low-cambered NACA 65-(c_l₀A10)06 airfoil sections. The blade chord was varied along the blade span to provide constant solidity. The blade designed for $\sigma = 0.5$ was also tested at $\sigma = 1.0$; however, since the blade was originally designed for $\sigma = 0.5$, it was not possible to obtain the exact design (free-vortex) condition. Since a compromise had to be made which resulted in the selection of a blade-setting angle for the design condition that was close to the stall angle of attack for each blade-setting angle, the

maximum efficiency and angle-of-attack range were adversely affected. The solidity was changed by varying the number of blades. For solidities of 0.5, 0.75, and 1.0 the number of blades was 13, 20, and 26, respectively. Three blade-setting angles were tested for each solidity: that is, at 4° above and at 4° below design as well as at the two-dimensional design angle of attack specified in reference 2. Typical vector diagrams for the mean station are shown in figures 1 to 3. The following table presents rotor design details for each solidity:

σ	Station	NACA airfoil section (a)	α_d , deg	θ_d , deg	β_{1d} , deg	β_{2d} , deg	ξ_d , deg	Radius, in.
0.5	Hub	65-(6A ₁₀)06	4.6	4.5	67.5	63.0	62.9	10.91
	Mean	65-(4A ₁₀)06	2.5	3.0	70.0	67.0	67.5	12.41
	Tip	65-(3A ₁₀)06	2.5	2.0	72.0	70.0	69.5	13.91
0.75	Hub	65-(5.6A ₁₀)06	4.5	6.1	67.5	61.5	63.0	10.91
	Mean	65-(4A ₁₀)06	3.0	4.0	70.0	66.0	67.0	12.41
	Tip	65-(3.2A ₁₀)06	2.1	2.9	72.0	70.1	69.9	13.91
1.0	Hub	65-(6A ₁₀)06	5.7	8.1	67.5	59.5	61.8	10.91
	Mean	65-(4A ₁₀)06	4.0	5.3	70.0	64.7	66.0	12.41
	Tip	65-(3A ₁₀)06	2.9	3.6	72.0	63.4	69.1	13.91

(a) The part of the designation of these sections within parentheses follows a system used explicitly for compressor and turbine profiles. In this system the number within the parentheses represents the design lift coefficient c_{l_0} in tenths. The letter A is identified with the mean line $a = 1.0$ and the subscript indicates the fraction (in tenths) of the lift coefficient associated with the particular mean line.

Each rotor was tested at low speeds in the 28-inch-diameter test compressor described in reference 3. Static pressure, total pressure, and flow angles were measured at 14 radial stations $1\frac{1}{2}$ inches ahead of and behind the rotor by using flow-survey instruments of the prism-probe types described in reference 4.

The turning angles measured are considered to be accurate to within $\pm\frac{1}{2}^\circ$. An indication of the accuracy of flow measurements can be obtained from the variation in mass flow across the rotor. (See fig. 4.) For all surveys the maximum difference is 4 percent, and the average variation is about 2 percent. Efficiencies and pressure-rise coefficients are believed to be accurate to within ± 3 percent.

RESULTS AND DISCUSSION OF ROTOR PERFORMANCE

Efficiency and Pressure-Rise Coefficients

Measured adiabatic efficiencies and pressure-rise coefficients were obtained from the instrument surveys and were mass weighted. These quantities are plotted against quantity-flow coefficients for each of the three blade-setting angles and solidities in figures 5, 6, and 7.

Satisfactory efficiencies were obtained over a moderate range of quantity-flow coefficients at each blade-setting angle. Maximum efficiencies of approximately 90 percent were obtained for solidities of 0.75 and 1.0 for all blade-setting angles. For a solidity of 0.5 maximum efficiencies of approximately 86 percent were obtained for the three blade-setting angles. For a solidity of 1.0 the efficiency was 80 percent or greater for ranges of flow coefficients of 0.06, 0.10, and 0.10 as the blade-setting angle decreased from $\xi_d + 4^\circ$ to $\xi_d - 4^\circ$. These flow coefficients correspond to ranges of angle of attack of approximately 4° , 5° , and 5° , respectively. At a solidity of 0.75 the ranges of flow coefficients for an efficiency of 80 percent or greater were 0.05, 0.11, and 0.15 as the blade-setting angle decreased from $\xi_d + 4^\circ$ to $\xi_d - 4^\circ$ with corresponding angle-of-attack ranges of 3.0° , 6.0° , and 7.5° . For a solidity of 0.5 the efficiency was 80 percent or more for flow-coefficient ranges of 0.10, 0.13, and 0.14 as the ranges of angle of attack were 5.0° , 8.0° , and 9.0° . For the same design inlet-angle conditions, the higher solidity exhibited a smaller angle-of-attack operating range for efficient operation.

Figure 8 is presented to show the typical variation of adiabatic efficiency across the annulus for the three solidities at angles of attack near design.

Variation of Section Turning Angle With Angle of Attack

Summaries of the variation of turning angle with angle of attack at three radii for three blade-setting angles are presented in figures 9, 10, and 11 for solidities of 0.5, 0.75, and 1.0, respectively. The three radii chosen were for an inboard section (radius, 11.41 inches), the mean section (radius, 12.41 inches), and an outboard section (radius, 13.41 inches). The inboard and outboard sections were almost 17 percent of the span from the inner and outer casings, respectively. These sections were selected in order to avoid the casing boundary-layer regions.

The rate of change of turning angle with angle of attack was, in general, about the same for each blade-setting angle but tended to

increase slightly with increasing solidity. The decrease in turning-angle range with increase of blade-setting angle was to be expected since, for a given turning angle, the static-pressure rise changes rapidly with changes in inlet angle. (See ref. 2.) Figure 9(a) ($\sigma = 0.5$) indicates that separation occurred prematurely on the inboard section at ξ_d and $\xi_d + 4^\circ$, and this premature separation accounts for the lower static rise and overall efficiency presented in figure 5. The same condition occurred at the outboard section for $\sigma = 0.75$ (fig. 10(c)). Although the curves for turning angle against angle of attack, in general, are typical of rotor performance, the useful operating range of the outboard section could have been increased slightly by decreasing the design angle of attack by approximately 2° . The estimated results from two-dimensional data (ref. 2) were within $\pm 2^\circ$ of the measured values of the rotor.

Comparison Between Low-Speed Rotor and Cascade Turning Angles

Figures 12, 13, and 14 present a detailed comparison of spanwise variations of measured turning angles and those estimated from cascade data for three angles of attack for each of three blade-setting angles and for each of three solidities. Cascade data were not extensive enough to provide estimated values for all of the solidity of 0.5; however, the estimated values that were available compare favorably with the measured values. For solidities of 0.75 and 1.0, the spanwise variation of the measured values was within 0.5° to 1.5° of the estimated values except near the inner and outer casing. The greatest deviation between measured and estimated values occurred near the tip. This difference is greater at the tip because of the thicker boundary layer and the rotor tip clearance. Both factors combine to give an increase in the effective angle of attack and turning angle.

Carpet Plots

Figure 15 presents rotor test data as cross plots of turning-angle data against air-inlet angle and angle of attack for the 0.4 camber mean section. For this figure the carpet-plot technique described in reference 5 was used. For each solidity, the angle-of-attack scales were shifted along the abscissa a number of scale units proportional to the changes in inlet angle. Combinations of angle of attack and inlet angle were shifted along the abscissa a number of scale units proportional to the changes in solidity. Lines of constant angle of attack and inlet angle have been drawn. Interpolations for intermediate angles of attack, air-inlet angles, and solidities can be made along the abscissa.

CONCLUSIONS

The turning angles, static- and total-pressure rise, and quantity flow were measured in a test compressor for three solidities over ranges of blade-setting angles, angles of attack, and air-inlet angles. The values obtained were compared with values estimated from two-dimensional data, and the following conclusions are made:

1. Turning angles estimated from two-dimensional data were within $\pm 2^\circ$ of the measured values of the rotor.
2. The rotor efficiency was satisfactory over a moderate range of quantity-flow coefficients at each blade-setting angle and for the three solidities.
3. Design angles of attack at high air-inlet angles must be accurately selected for maximum efficiency and angle-of-attack range.

Langley Aeronautical Laboratory,
National Advisory Committee for Aeronautics,
Langley Field, Va., May 21, 1958.

REFERENCES

1. Herrig, L. Joseph, Emery, James C., and Erwin, John R.: Systematic Two-Dimensional Cascade Tests of NACA 65-Series Compressor Blades at Low Speeds. NACA TN 3916, 1957. (Supersedes NACA RM L51G31.)
2. Emery, James C.: Low-Speed Cascade Investigation of Thin Low-Camber NACA 65-Series Blade Sections at High Inlet Angles. NACA RM L57E03, 1957.
3. Schulze, Wallace M., Erwin, John R., and Ashby, George C., Jr.: NACA 65-Series Compressor Rotor Performance With Varying Annulus-Area Ratio, Solidity, Blade Angle, and Reynolds Number and Comparison With Cascade Results. NACA TN 4130, 1957. (Supersedes NACA RM L52L17.)
4. Schulze, Wallace M., Ashby, George C., Jr., and Erwin, John R.: Several Combination Probes for Surveying Static and Total Pressure and Flow Direction. NACA TN 2830, 1952.
5. Felix, A. Richard: Summary of 65-Series Compressor-Blade Low-Speed Cascade Data by Use of the Carpet-Plotting Technique. NACA TN 3913, 1957. (Supersedes NACA RM L54H18a.)

NACA 65-(4A₁₀)06 blade section

$\alpha_d = 2.5^\circ$
 $\theta_d = 3^\circ$

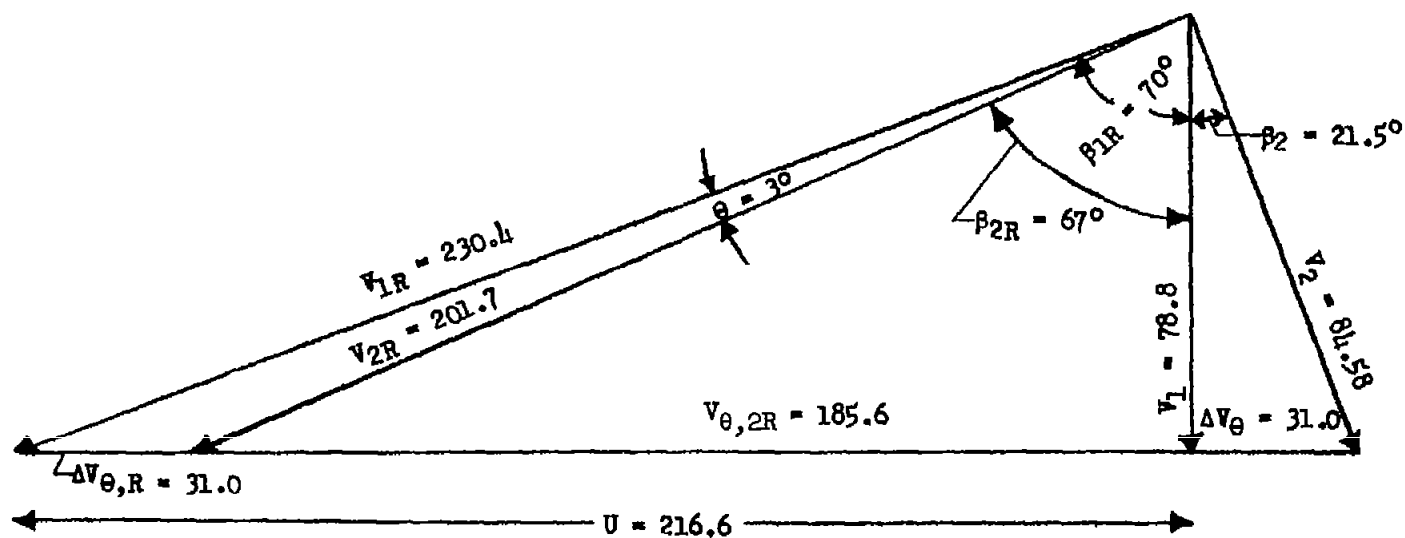
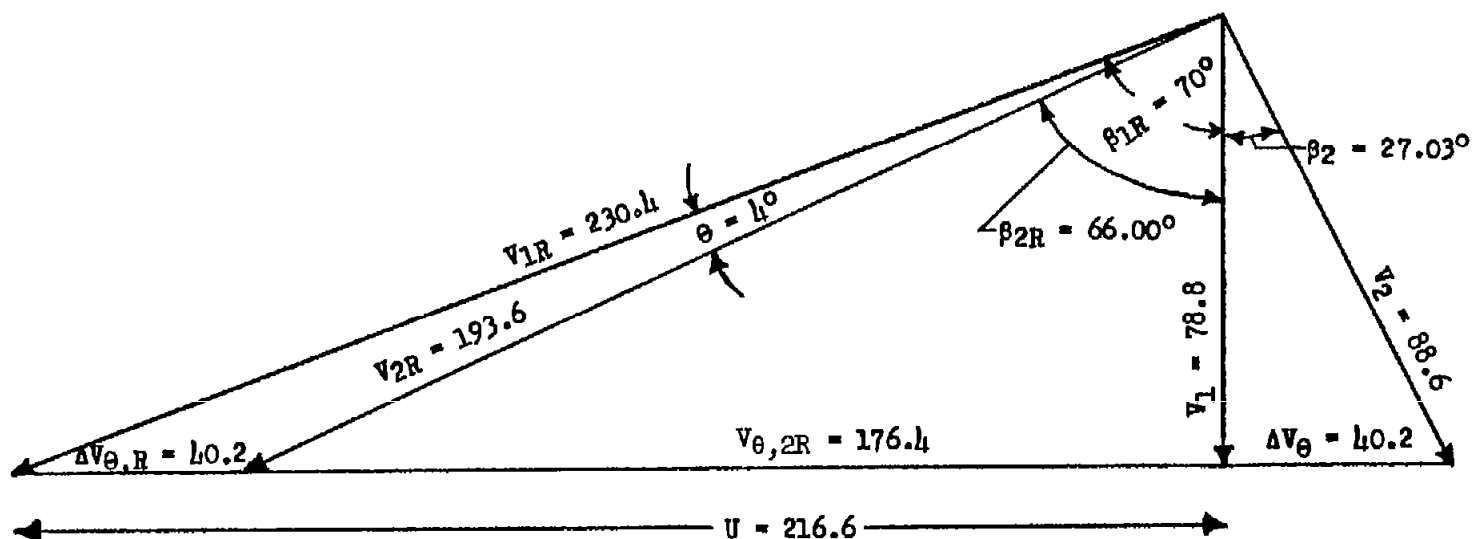


Figure 1.- Mean-section vector diagram. Free-vortex-flow condition; $\sigma = 0.5$.

NACA 65-(4A₁₀)06 blade section $\alpha_d = 3^\circ$ $\theta_d = 4^\circ$ Figure 2.- Mean-section vector diagram. Free-vortex-flow condition; $\sigma = 0.75$.

NACA 65-(4A₁₀)06 blade section

$\alpha_d = 4.0^\circ$

$\theta_d = 5.3^\circ$

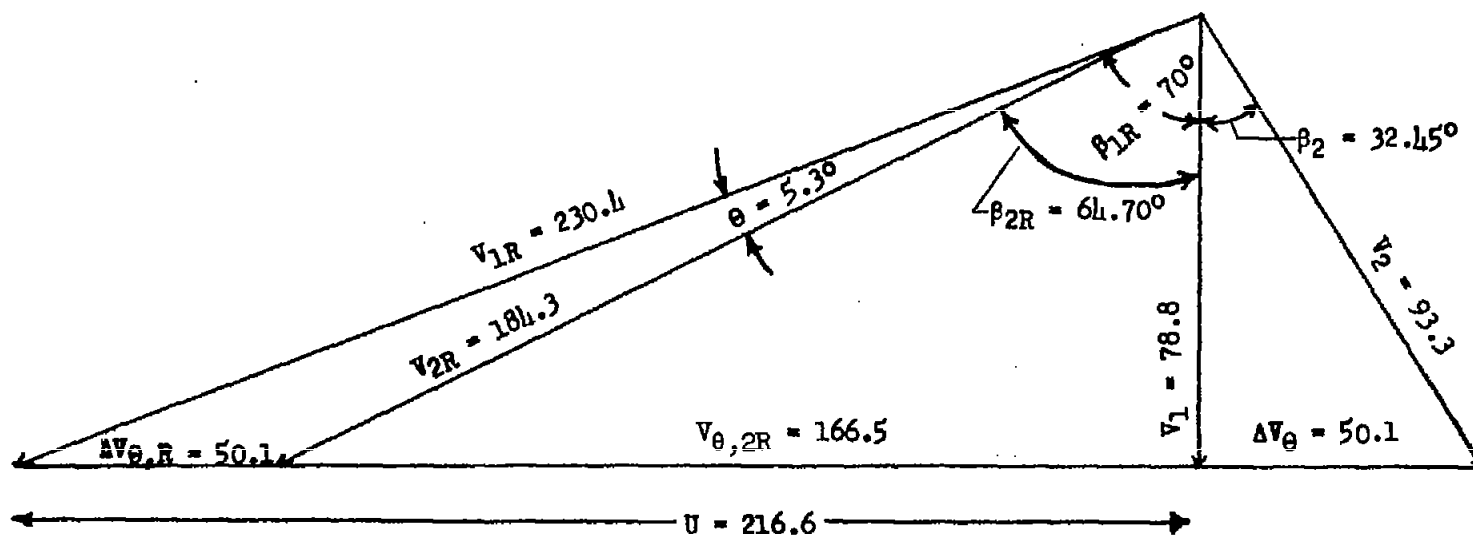


Figure 3.- Mean-section vector diagram. Free-vortex-flow condition; $\sigma = 1.0$.

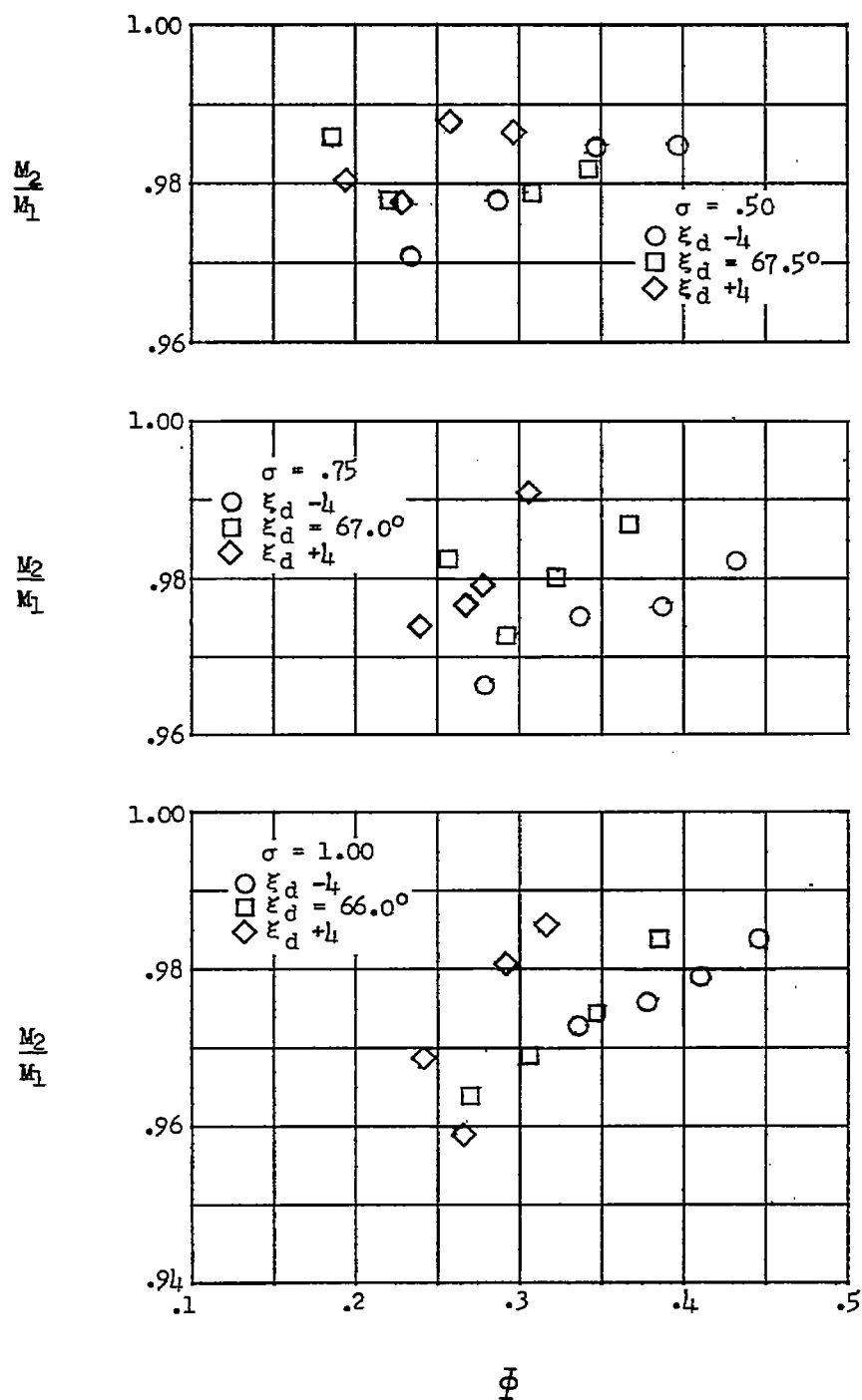


Figure 4.- Variation in mass flow as measured upstream and downstream of compressor rotor.

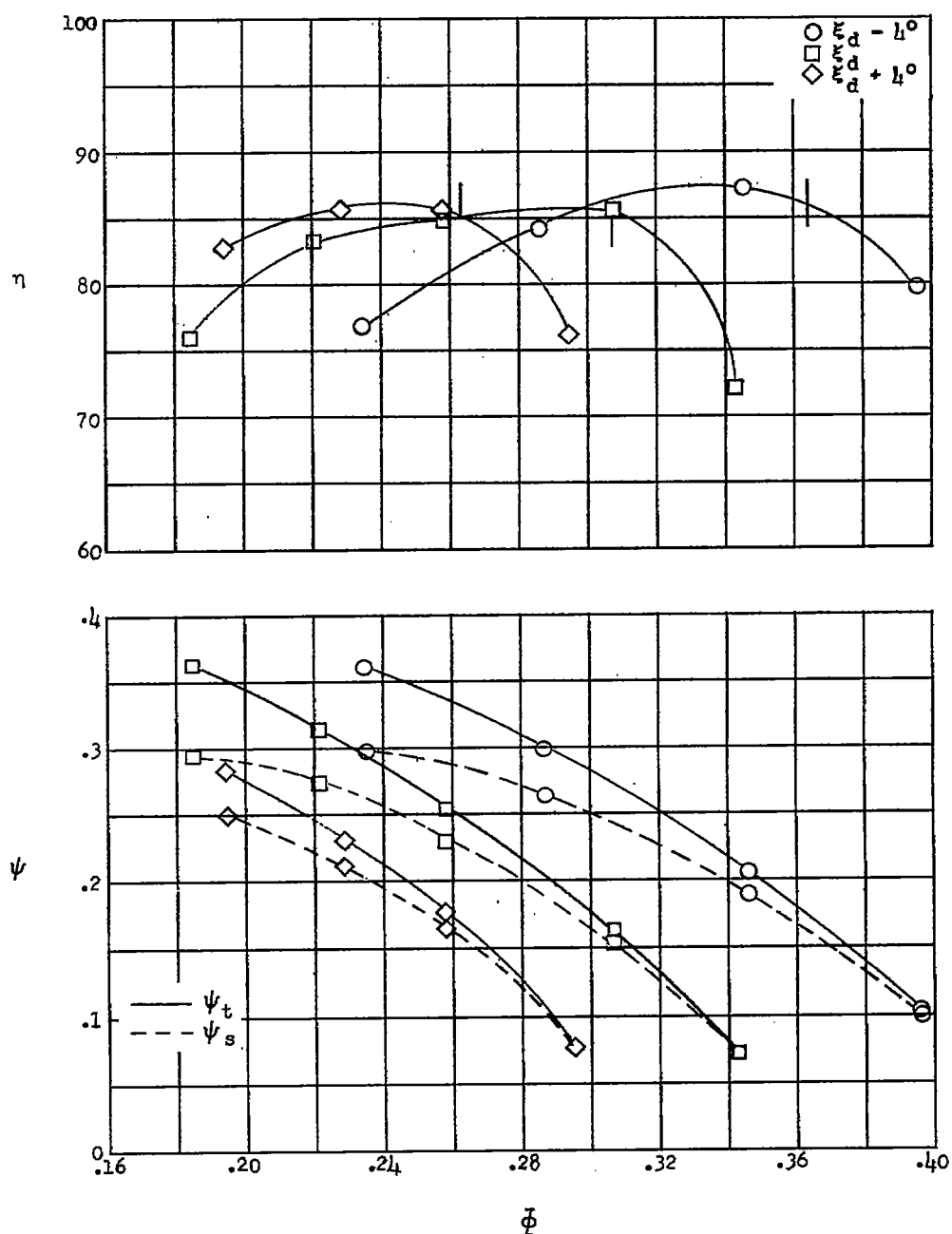


Figure 5.- Variation of adiabatic efficiency and total- and static-pressure-rise coefficients with quantity-flow coefficients at three blade-setting angles, $\sigma = 0.5$, and $\xi_d = 67.5^\circ$. Vertical lines across curve indicate design angle of attack.

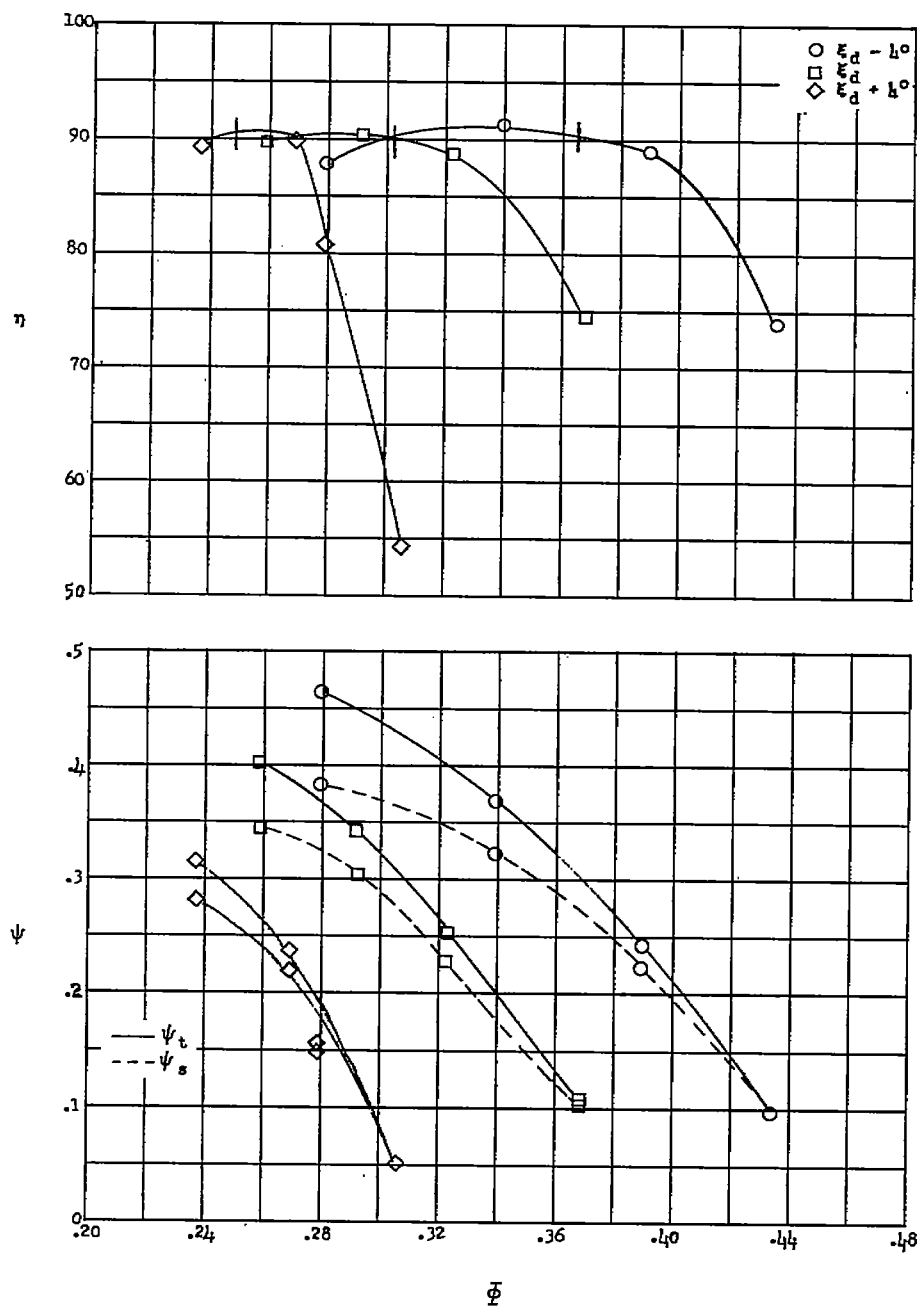


Figure 6.- Variation of adiabatic efficiency and total- and static-pressure-rise coefficients with quantity-flow coefficients at three blade-setting angles, $\sigma = 0.75$, and $\xi_d = 67.0^\circ$. Vertical lines across curve indicate design angle of attack.

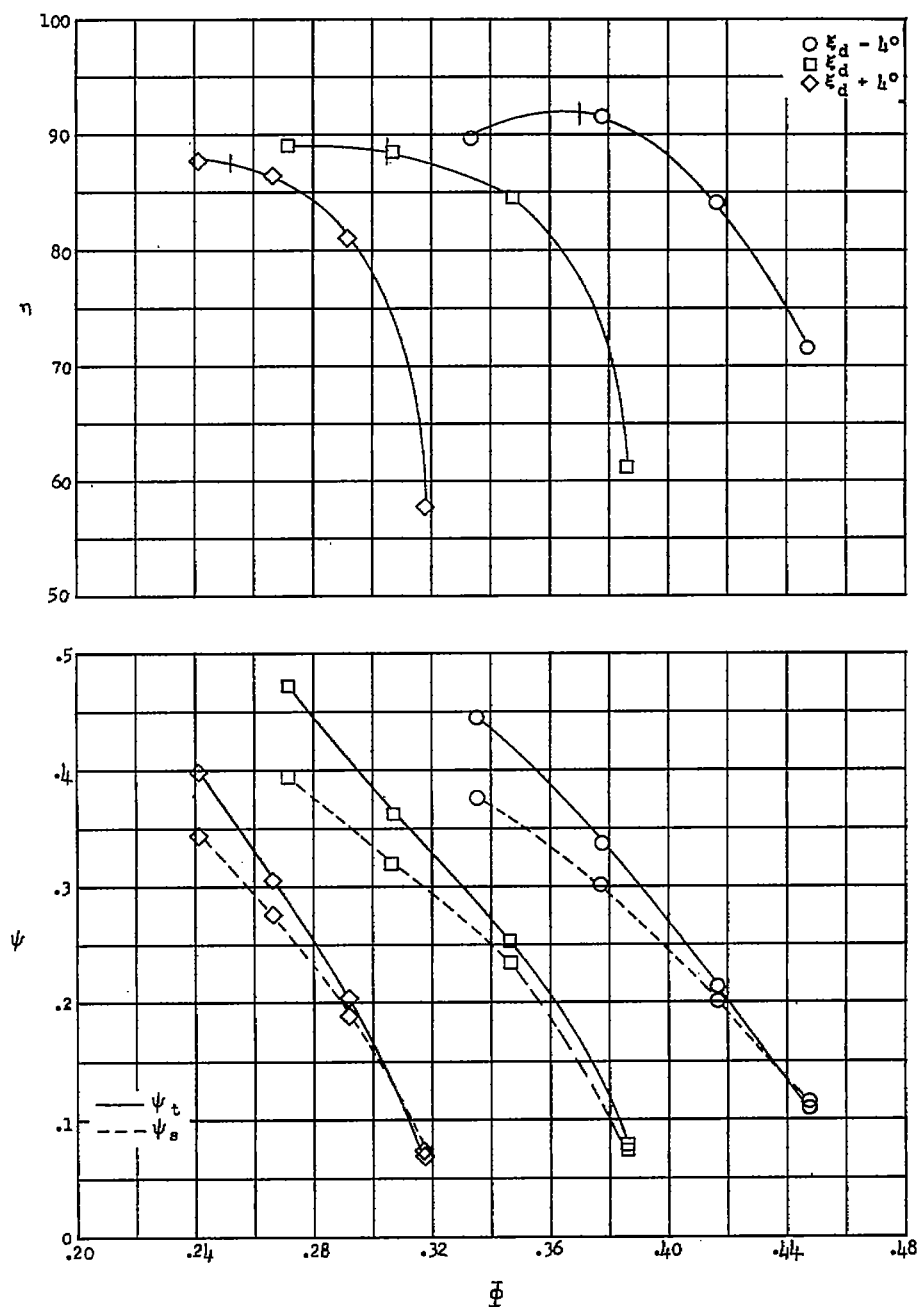


Figure 7.- Variation of adiabatic efficiency and total- and static-pressure-rise coefficients with quantity-flow coefficients at three blade-setting angles, $\sigma = 1.0$, and $\xi_d = 66.0^\circ$. Vertical lines across curve indicate design angle of attack.

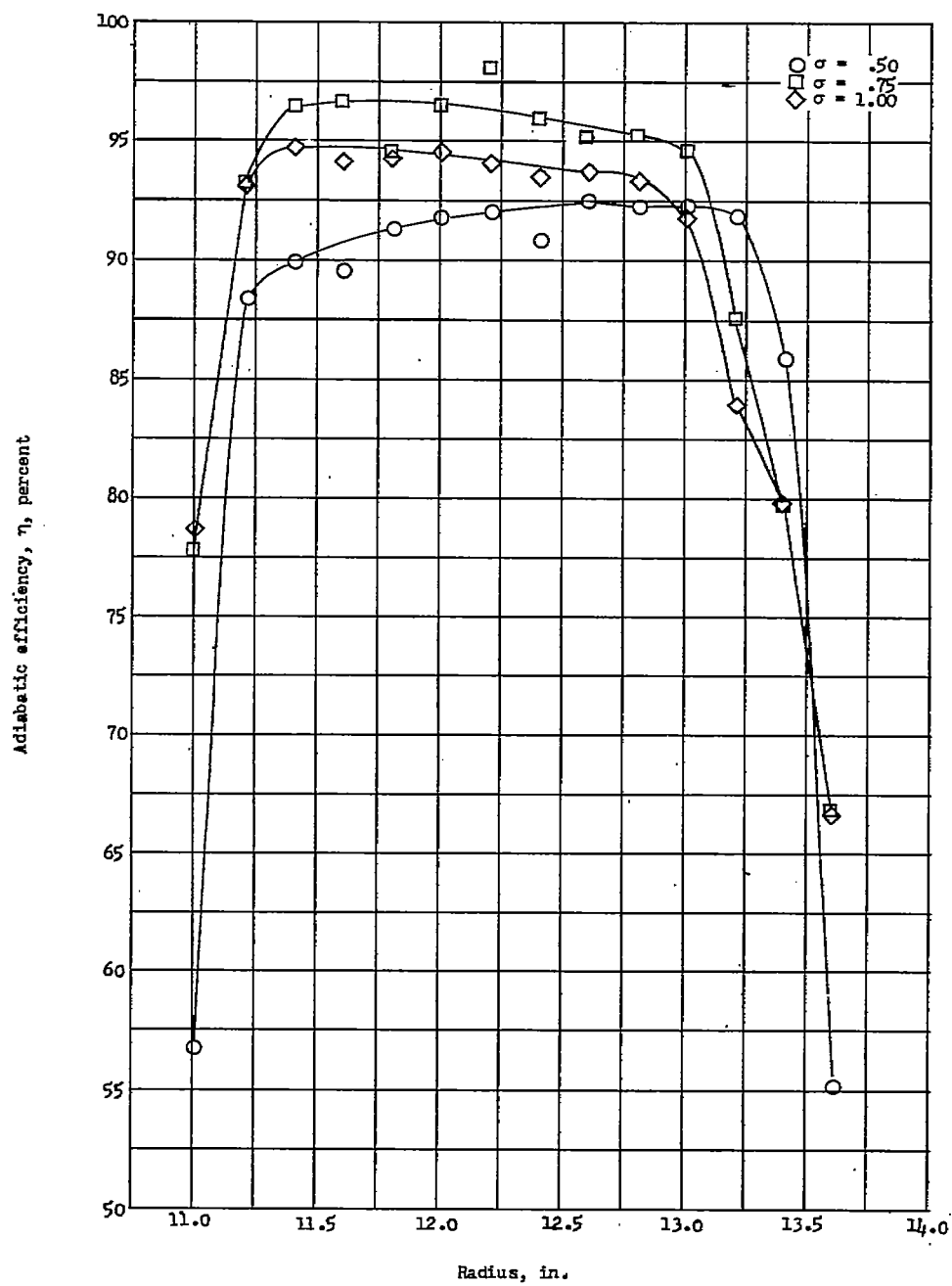
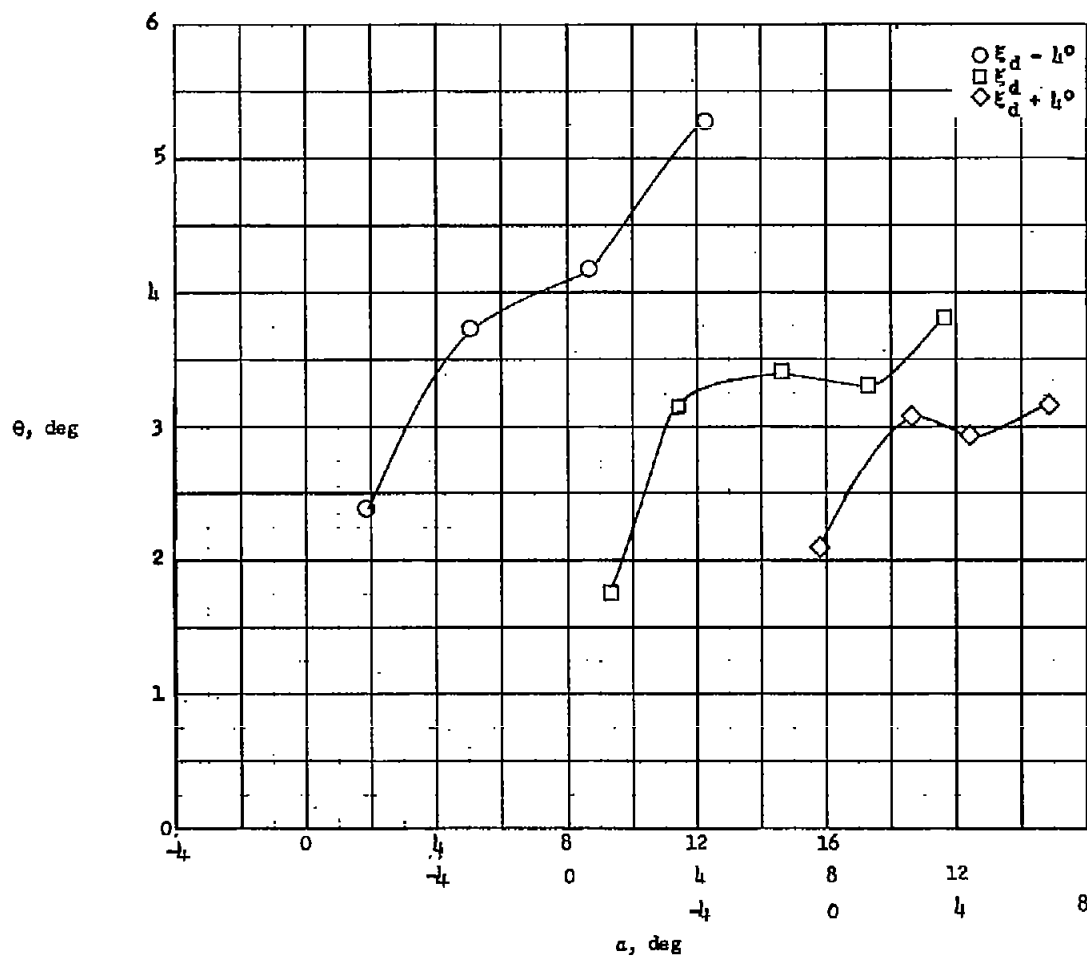
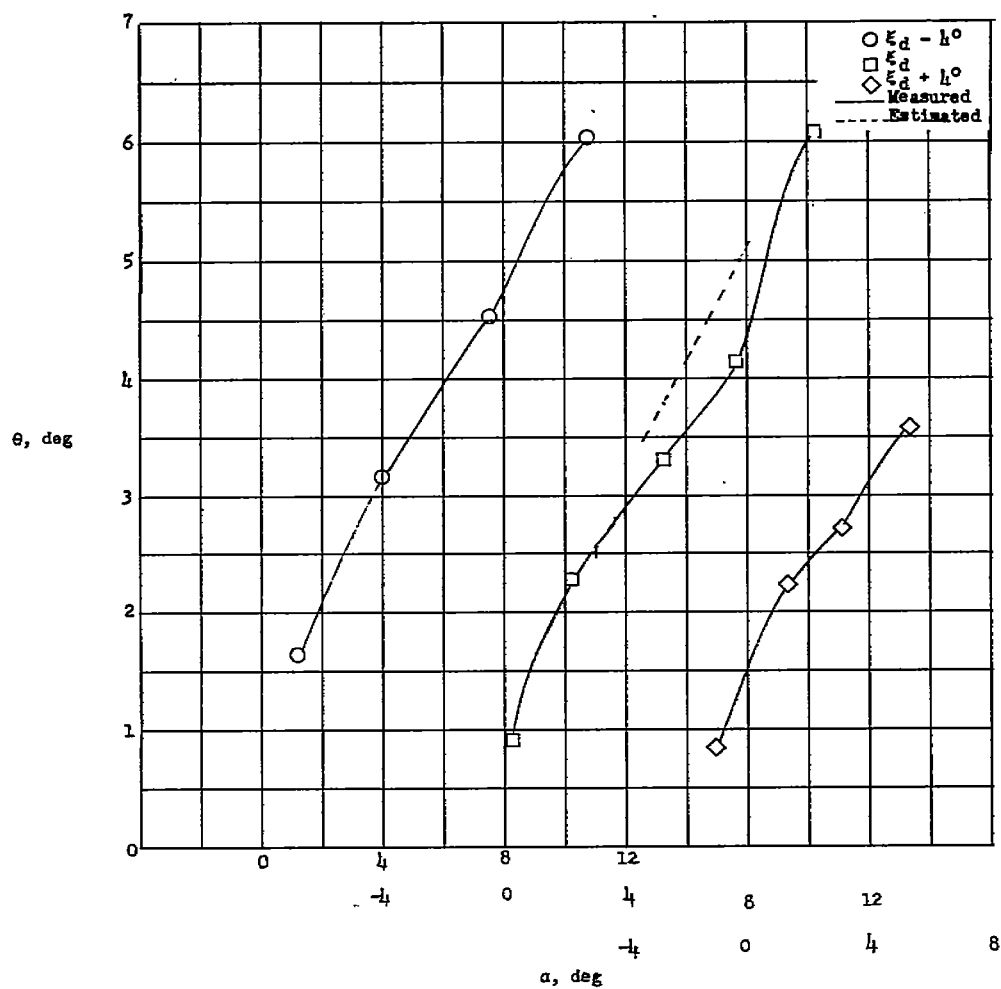


Figure 8.- Measured blade-element efficiencies across the annulus at solidities of 0.5, 0.75, and 1.0 near design angle of attack.



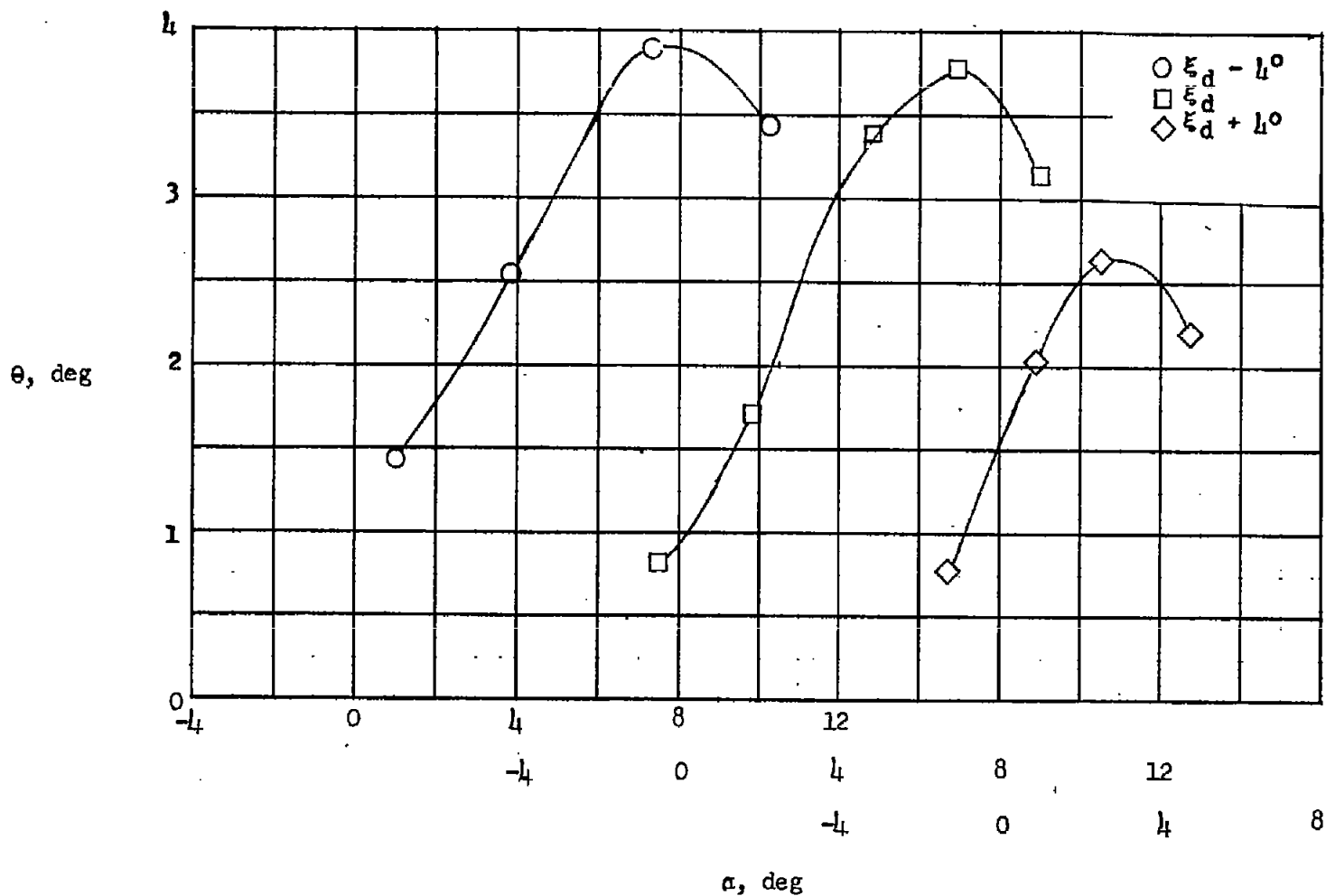
(a) Inboard section; NACA 65-(3.3A₁₀)06 section; radius, 11.41 inches; $\theta_d = 67.5^\circ$.

Figure 9.- Variation of measured and estimated turning angles with angle of attack for three radii and for three blade-setting angles. $\sigma = 0.5$.



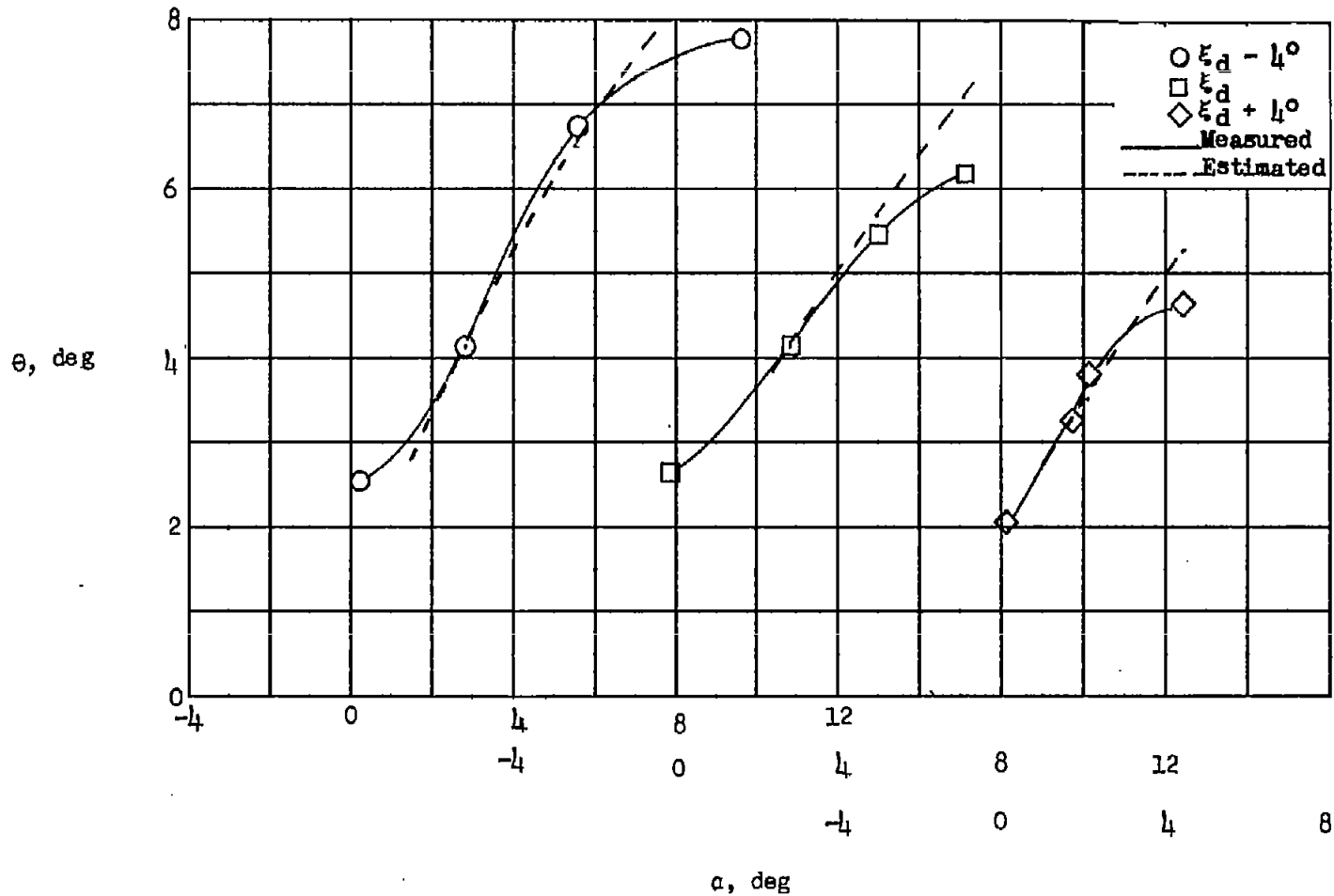
(b) Mean section; NACA 65-(4A₁₀)06 section; radius, 12.41 inches; $\xi_d = 67.5^\circ$.

Figure 9.- Continued.



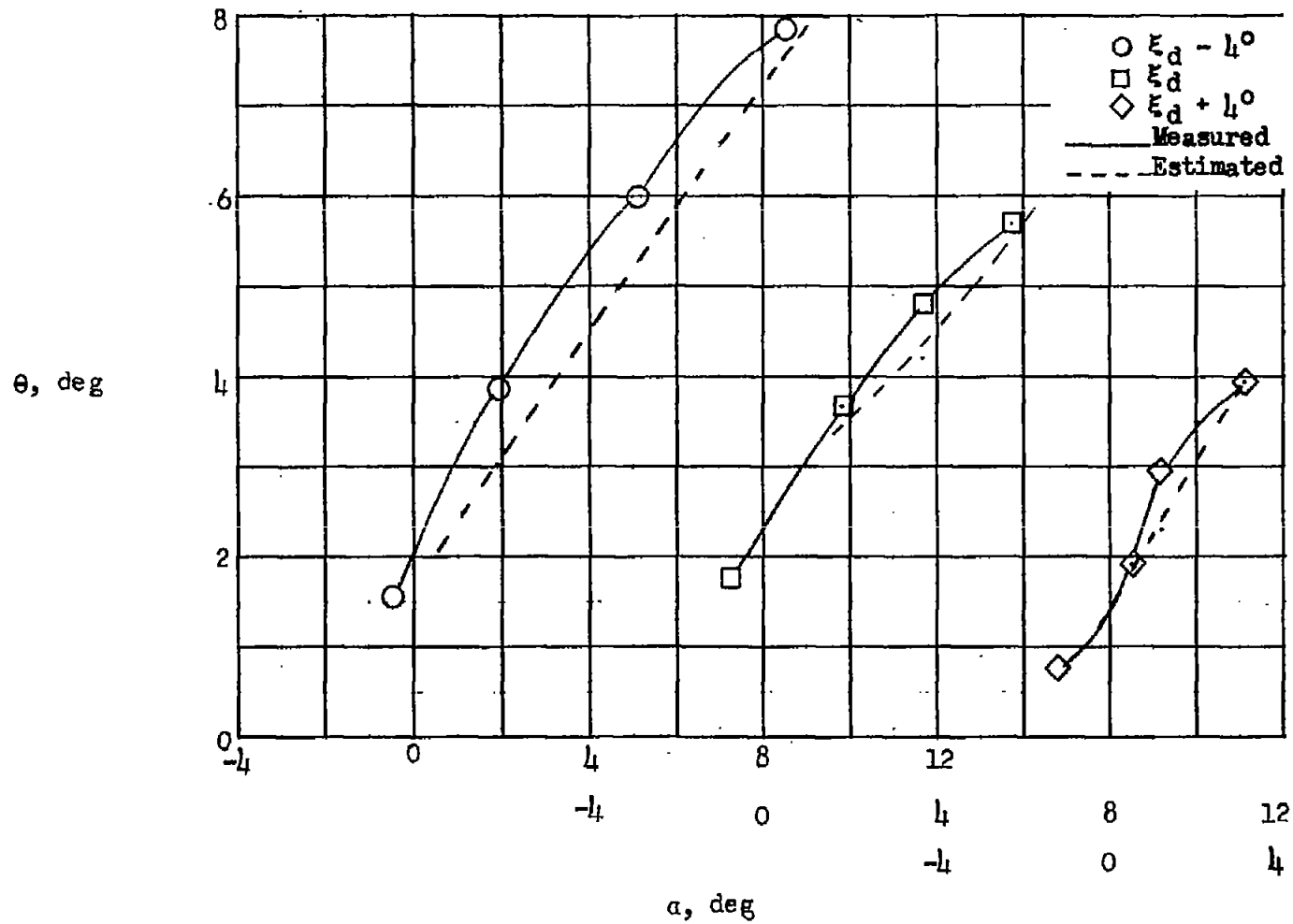
(c) Outboard section; NACA 65-(5.3A₁₀)06 section; radius, 13.41 inches; $\delta_d = 67.5^\circ$.

Figure 9.- Concluded.



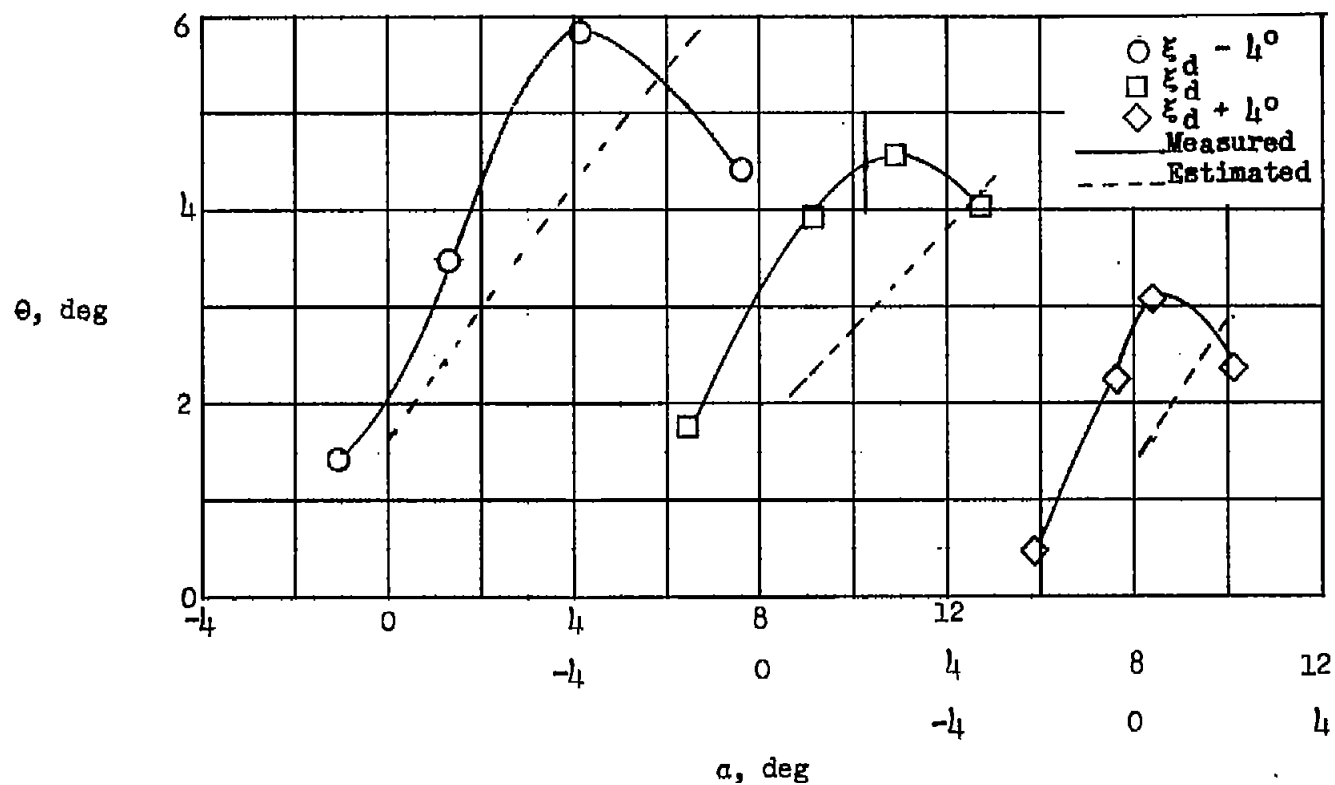
(a) Inboard section; NACA 65-(5A₁₀)06 section; radius, 11.41 inches; $\xi_d = 67.0^\circ$.

Figure 10.- Variation of measured and estimated turning angles with angle of attack for three radii and for three blade-setting angles. $\sigma = 0.75$.



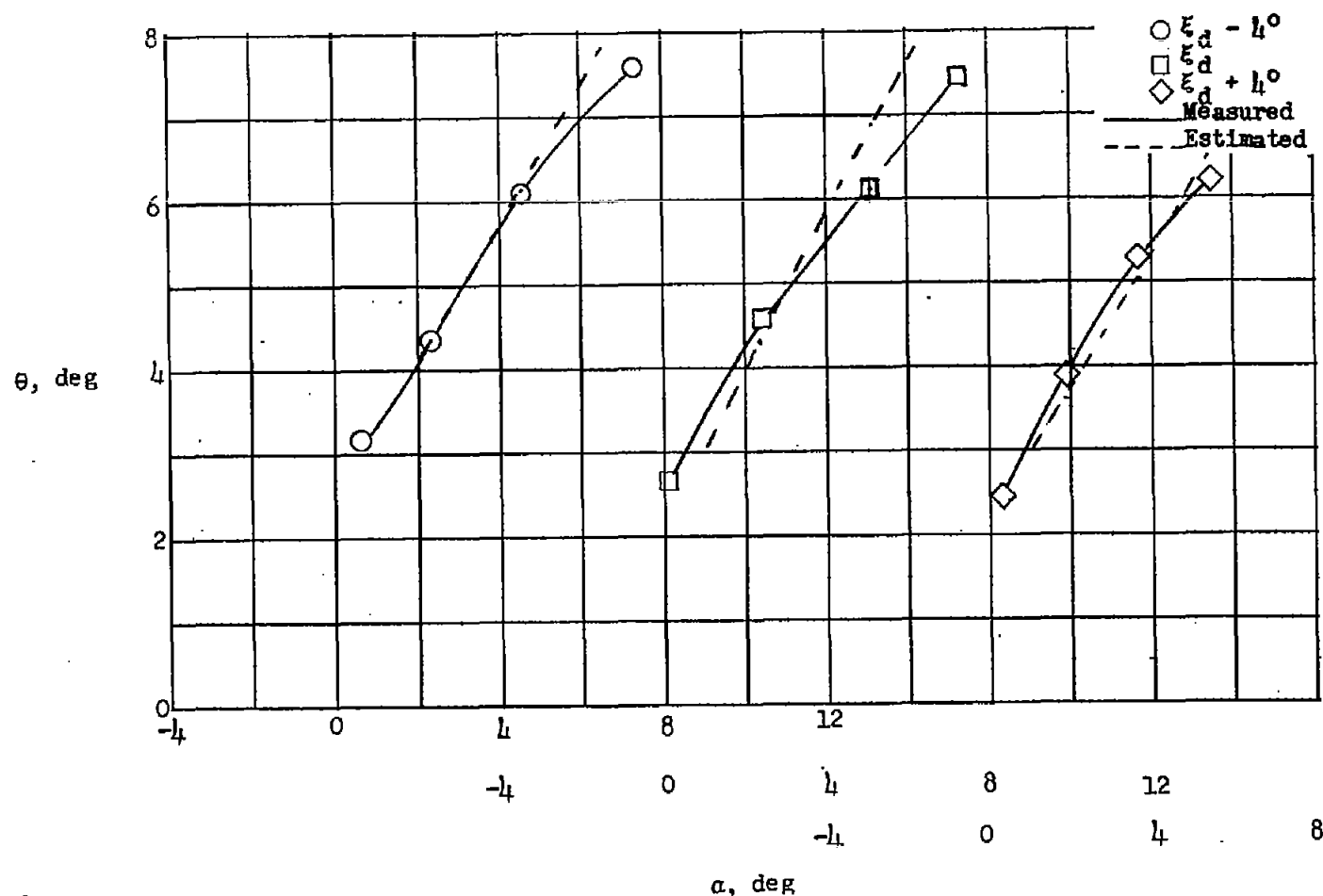
(b) Mean section; NACA 65-(4A₁₀)06 section; radius, 12.41 inches; $\xi_d = 67.0^\circ$.

Figure 10.- Continued.



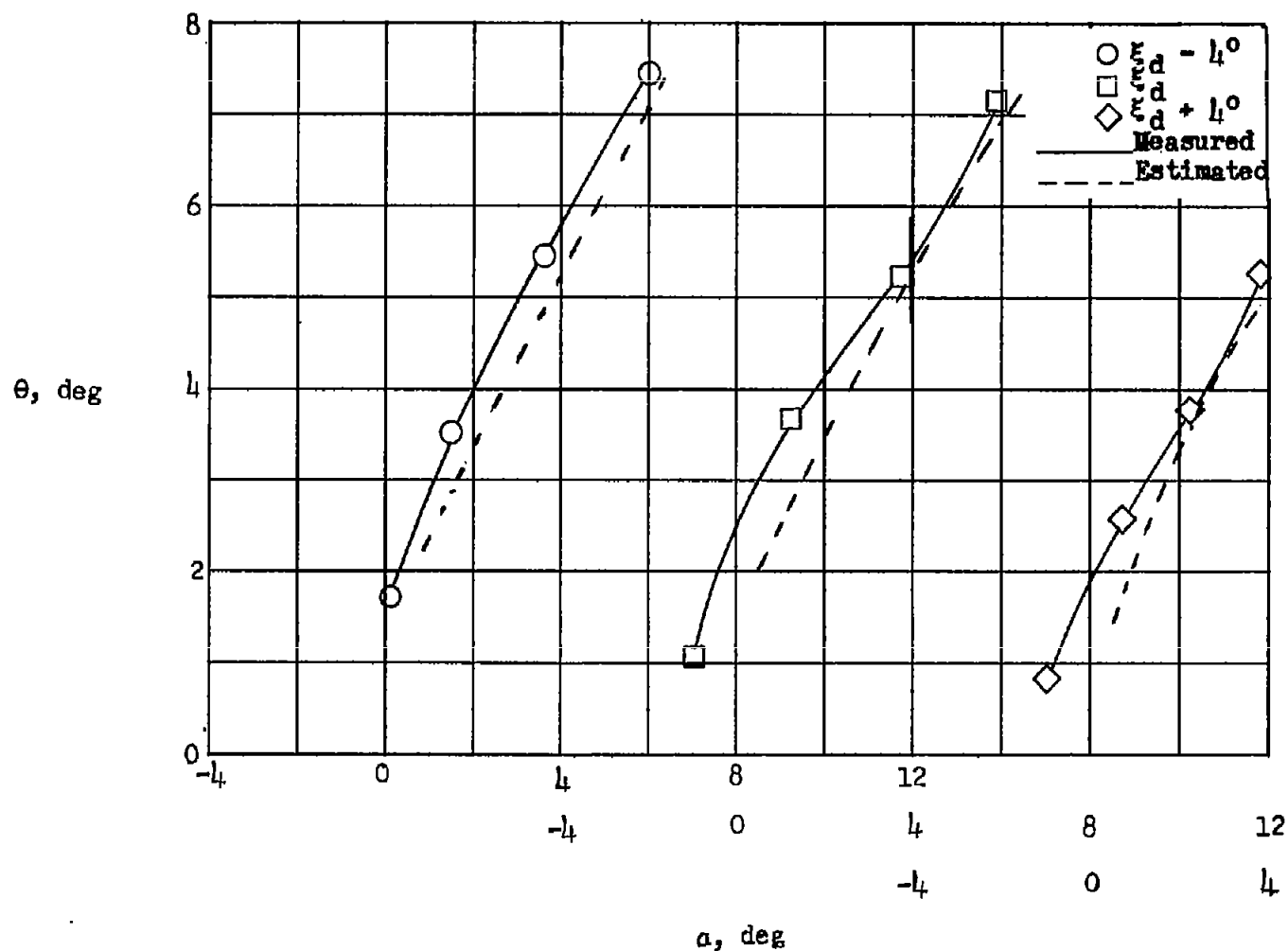
(c) Outboard section; NACA 65-(3.5A₁₀)06 section; radius, 13.41 inches; $\xi_d = 67.0^\circ$.

Figure 10.- Concluded.



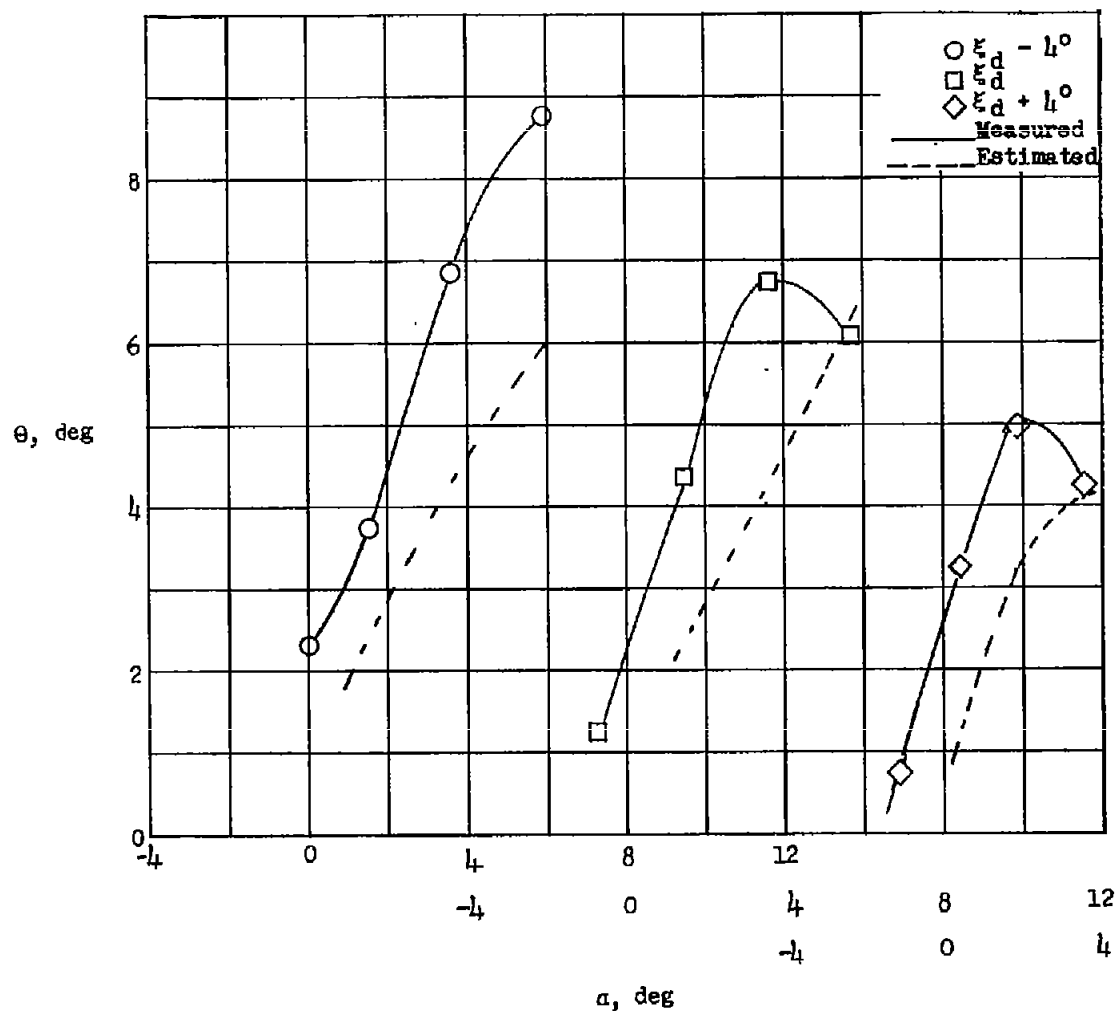
(a) Inboard section; NACA 65-(3.3A₁₀)06 section; radius, 11.41 inches; $\xi_d = 66.0^\circ$.

Figure 11.- Variation of measured and estimated turning angles with angle of attack for three radii and for three blade-setting angles. $\sigma = 1.0$.



(b) Mean section; NACA 65-(4A₁₀)06 section; radius, 12.41 inches; $\epsilon_d = 66.0^\circ$.

Figure 11.- Continued.



(c) Outboard section; NACA 65-(5.3A₁₀)06 section; radius, 13.41 inches; $\xi_d = 66.0^\circ$.

Figure 11.- Concluded.

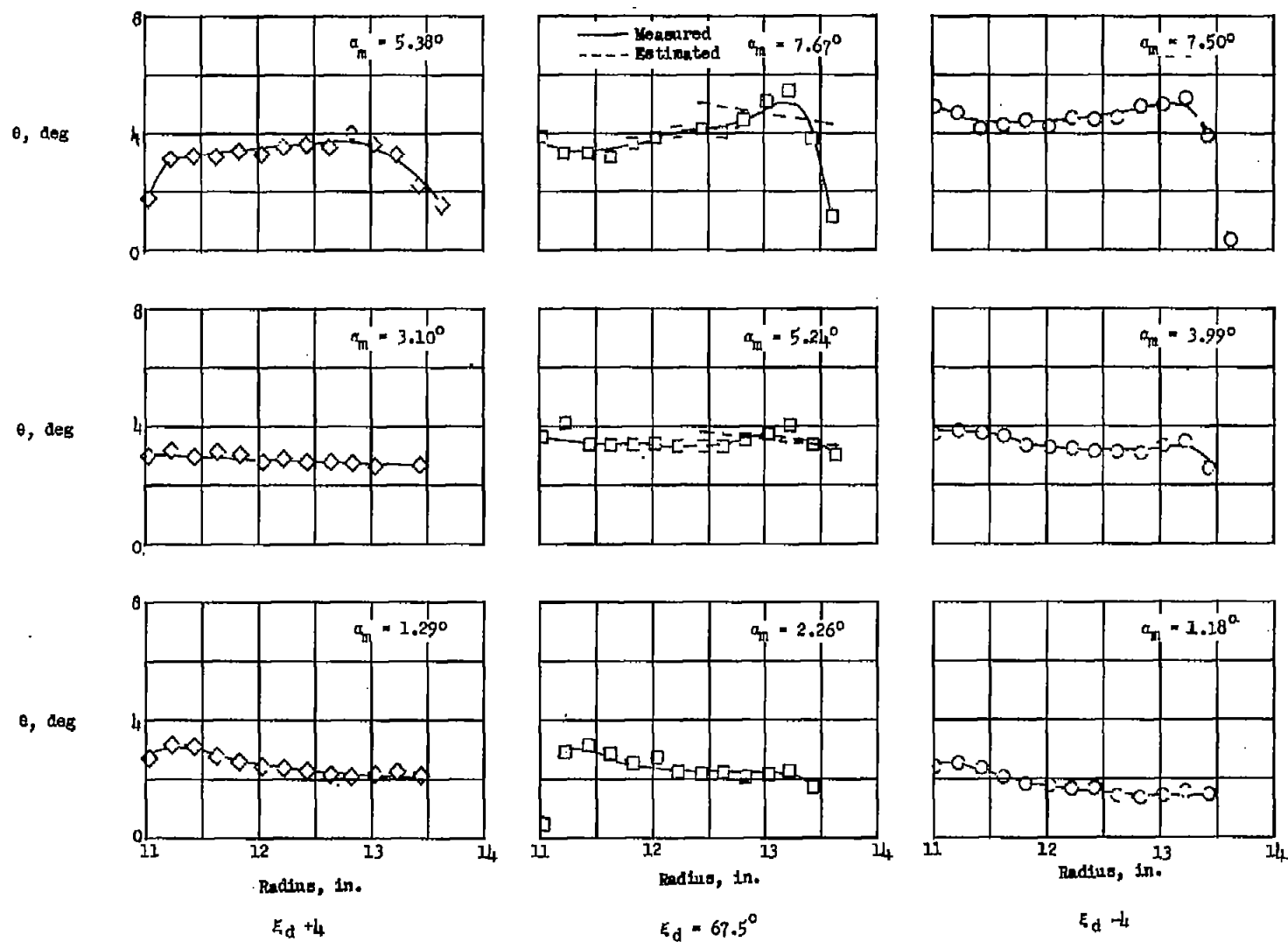


Figure 12.- Radial variation of measured and estimated turning angles for three angles of attack and for three blade-setting angles. $\sigma = 0.5$; $\alpha_{d,m} = 2.5^\circ$.

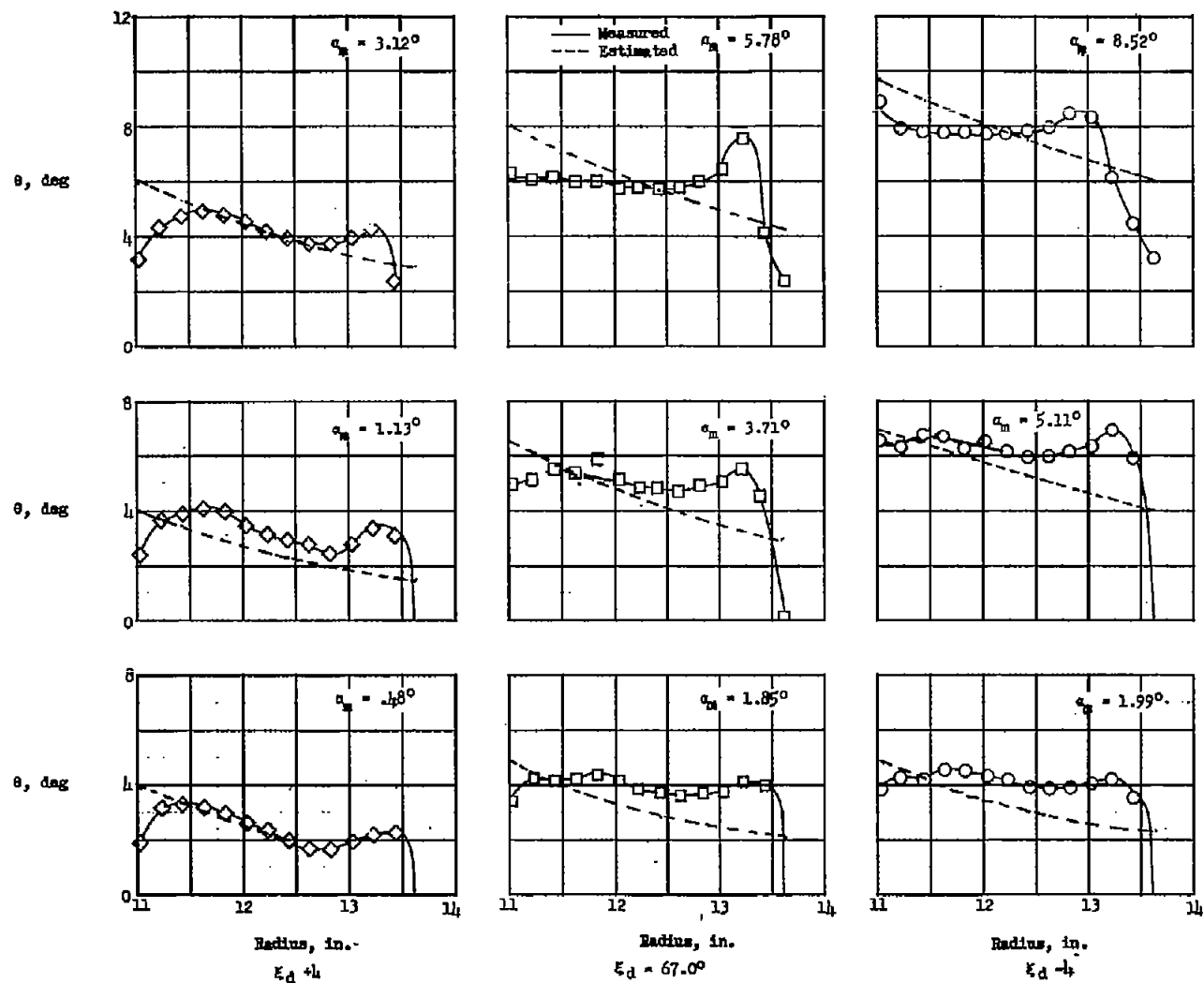


Figure 13.- Radial variation of measured and estimated turning angles for three angles of attack and for three blade-setting angles. $\sigma = 0.75$; $\alpha_{d,m} = 3.0^\circ$.

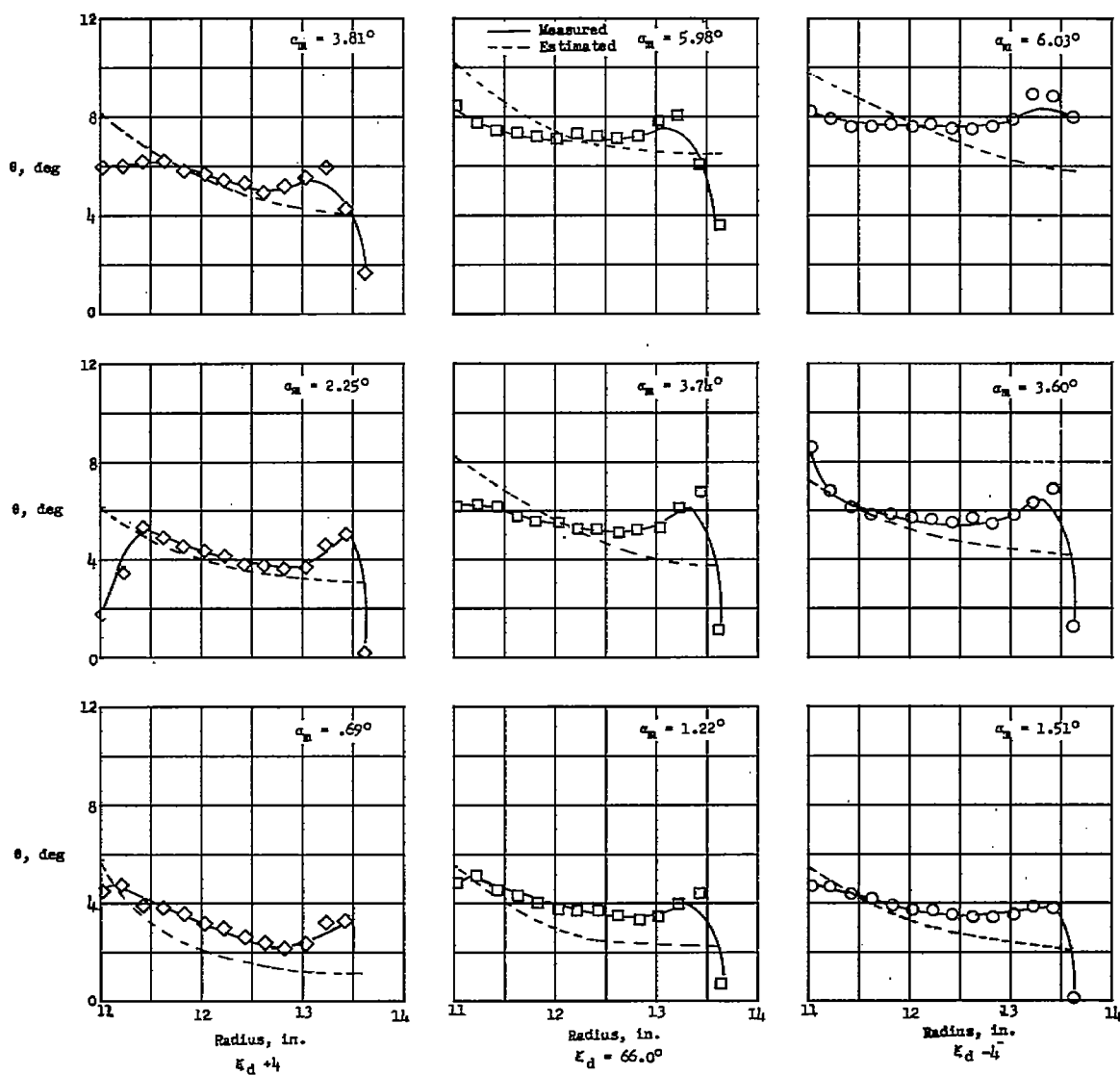


Figure 14.- Radial variation of measured and estimated turning angles for three angles of attack and for three blade-setting angles.
 $\sigma = 1.0$; $\alpha_{d,m} = 4.0^\circ$.

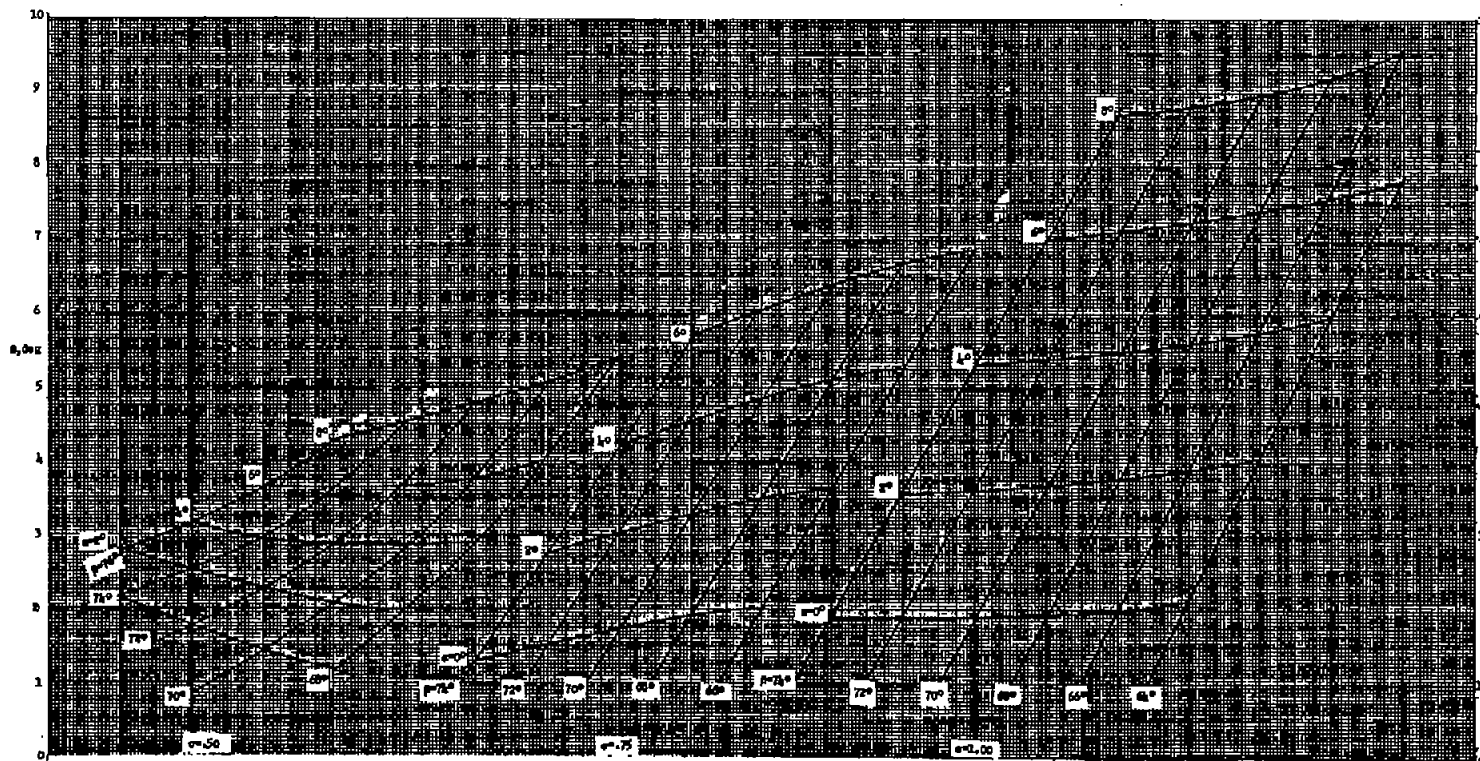


Figure 15.- Variation of turning angle, angle of attack, and air-inlet angle for solidities of 0.50, 0.75, and 1.00 at the mean section. $c_{l0} = 0.4$.